Nucleic Acids Research, 2005, Vol. 33, No. 13 ***e123***
doi:10.1093/nar/gni125

An ultrasensitive photoelectrochemical nucleic acid biosensor

Zhiqiang Gao[1,2,*] and Natalia C. Tansil[1,2]

[1]Institute of Bioengineering and Nanotechnology, 31 Biopolis Way, Singapore 138669 and [2]School of Materials Science and Engineering, Nanyang Technological University, Singapore 639798

Received May 8, 2005; Revised July 5, 2005; Accepted July 18, 2005

ABSTRACT

A simple and ultrasensitive procedure for non-labeling detection of nucleic acids is described in this study. It is based on the photoelectrochemical detection of target nucleic acids by forming a nucleic acid/photoreporter adduct layer on an ITO electrode. The target nucleic acids were hybridized with immobilized oligonucleotide capture probes on the ITO electrode. A subsequent binding of a photoreporter—a photoactive threading *bis*-intercalator consisting of two *N,N′-bis*(3-propyl-imidazole)-1,4,5,8-naphthalene diimides (PIND) linked by a $Ru(bpy)_2^{2+}$ (bpy = 2,2′-bipyridine) complex (PIND–Ru–PIND)—allowed for photoelectrochemical detection of the target nucleic acids. The extremely low dissociation rate of the adduct and the highly reversible photoelectrochemical response under visible light illumination (490 nm) make it possible to conduct nucleic acid detection, with a sensitivity enhancement of four orders of magnitude over voltammetry. These results demonstrate for the first time the potential of photoelectrochemical biosensors for PCR-free ultrasensitive detection of nucleic acids.

INTRODUCTION

Over the past decade, there have been significant advances in the development of nucleic acid biosensors based on the immobilization of short oligonucleotide capture probes onto a solid support to form a biorecognition layer and for the subsequent detection of sample nucleic acids hybridized to the capture probes. The most popular methods rely on the use of fluorescent materials in an array format (microarray) (1). Most of the fluorescent microarray assays are performed in conjunction with solution phase (off-chip) preamplification/labeling approaches such as PCRs (2). They offer the highest degree of sensitivity and the widest dynamic range. However, PCR amplification does not avoid the difficulties that originate from the inherent nature of the technique. Its amplification power may dramatically be affected by small variations in experimental conditions and sample composition. Optimization of the complicated primers and experimental conditions for each specific gene is a formidable task. Very frequently, genes may not be represented at the same levels in the final PCR products due to the selective and nonlinear target amplification (3). Incomplete denaturation of the nucleic acid's secondary structure during the cDNA synthesis step can also halt the polymerase, resulting in shorter cDNA copies of target genes. PCR-based methods are of limited applicability in quantifying nucleic acids of high complexity because the PCR products of the amplification are likely to interfere with each other, resulting in loss of amplification efficiency and specificity (4). Off-chip target amplification approaches also significantly increase the cost of the procedures and often lead to sequence-dependent quantification bias. To address these drawbacks, several strategies such as the rolling circle amplification (4), branched DNA technology (5), catalyzed reporter deposition (6), dendritic tags (7), enzymatic amplification (8–10) and chemical amplification (11–14) have been proposed. Among them, electronic transduction methods have the potential to provide a simple, accurate and inexpensive platform for ultrasensitive nucleic acid assays because of the inherent miniaturization of electronic devices and their compatibility with the advanced semiconductor technologies. It has been demonstrated that as few as 10^3 copies/sample of genes can be directly detected electrochemically without biochemical amplification (8–10). This high-performance assays promise to be attractive alternatives for the quantification of gene expression and clinical diagnostics.

In this report, we extend the scope of electronic transduction to photoelectrochemistry. The threading *bis*-intercalator, *N,N′-bis*(3-propyl-imidazole)-1,4,5,8-naphthalene diimides (PIND) linked by a $Ru(bpy)_2^{2+}$ (bpy = 2,2′-bipyridine) complex (PIND–Ru–PIND), was employed in ultrasensitive non-labeled detection of nucleic acid hybridization events. A remarkable sensitivity enhancement was achieved when compared with direct voltammetric detection.

*To whom correspondence should be addressed. Tel: +65 6824 7113; Fax: +65 6478 9084; Email: zqgao@ibn.a-star.edu.sg

A photoelectrochemical signal was observed when as little as femtomolar nucleic acid was present. To our knowledge, these experiments comprise the first example of photoelectrochemical approach for detecting nucleic acids. The sensitivity of the biosensor is among the highest ones reported. Further improvements in the sensitivity and the specificity of the approach can be achieved by designing a more selective photoreporter, optimizing hybridization conditions and further minimizing the background noise caused by non-hybridization- related uptake of the intercalator and electromagnetic interference. Thus the photoelectrochemical amplification offers a potentially powerful approach to hybridization-based nucleic acid biosensors.

MATERIALS AND METHODS

Reagents

1(3-Aminopropyl)-imidazole (98%), 1,4,5,8-naphthalene tetracarboxylic dianhydride (>95%), SDS (>99%), sodium borohydride (>99%) and 11-aminoundecanoic acid (AUA, >99%) were purchased from Sigma–Aldrich (St Louis, MO). $Ru(bpy)_2Cl_2$ (99%) was purchased from Avocado Research Chemicals Ltd (Leysham, Lancester, UK). YOYO-3, a dimer of oxazole yellow, was purchased from Molecular Probes (Eugene, OR). All other reagents were obtained from Sigma–Aldrich and used without further purification. Aldehyde-modified oligonucleotide capture probes used in this work were custom-made by Invitrogen Corporation (Carlsbad, CA) and all other oligonucleotides of PCR purity were custom-made by 1st Base Pte Ltd (Singapore). Oligonucleotide sequences used in this work were as follows: 5′-CAT TCC GTA GAA TCC AGG GAA GCG TGT CAC-3′ (synthetic target nucleic acid), 5′-OHC-$(CH_2)_6$-A_6-GTG ACA CGC TTC CCT GGA TTC TAC GGA ATC-3′ (capture probe for synthetic nucleic acid), 5′-OHC-$(CH_2)_6$-A_6-CCT CTC GCG AGT CAA CAG AAT GCT TAA CAT-3′ (capture probe for control biosensor), 5′-OHC-$(CH_2)_6$-A_6-ATG GAG GAT TCA CAG TCG GA-3′ (capture probe 1 for TP53 cDNA and mRNA, sense) and 5′-OHC-$(CH_2)_6$-A_6-TCA GTC TGA GTC AGG CCC CA-3′ (capture probe 2 for TP53 cDNA, antisense). A 10 mM Tris–HCl, 1.0 mM EDTA and 0.10 M NaCl (TE) buffer solution was used as the hybridization buffer.

Apparatus

Electrochemical experiments were carried out using a CH Instruments model 660A electrochemical workstation (CH Instruments, Austin, TX). A conventional three-electrode system, consisting of the ITO working electrode (0.20 ± 0.02 cm^2), a non-leak Ag/AgCl (3.0 M NaCl) reference electrode (Cypress Systems, Lawrence, KS) and a platinum wire counter electrode, was used in all electrochemical measurements. UV-visible and fluorescence spectra were recorded on a V-570 UV/VIS/NIR spectrophotometer (JASCO Corp., Japan) and a Fluorolog®-3 spectrofluorometer (Jobin Yvon Inc., Edison, NJ), respectively. Measurements of photocurrent were performed with the spectrofluorometer in conjunction with a synchronized 660A electrochemical workstation. The discovery mode of the spectrofluorometer was adopted for photocurrent action experiments at 10 nm interval. The intensity of the monochromatic light incident on the ITO electrode was controlled by adjusting both the slit width and the distance from the illuminator. The light intensity at 490 nm was calibrated by a Newport model 841-PE energy and power meter (Newport Corp., Irvine, CA). Illumination was performed from the front of the ITO electrode to prevent the absorption of light by the glass substrate. The three electrodes were hosted in a standard 1.0 cm fluorescence cuvette and arranged in such a way that the working electrode faces the illumination window and the other two electrodes are behind the working electrode. All potentials reported in this work were referred to the Ag/AgCl electrode. All experiments were carried out at room temperature, unless otherwise stated.

Synthesis of PIND–Ru–PIND

The synthesis of PIND–Ru–PIND is outlined in Scheme 1. PIND was prepared following a procedure described previously (11). PIND–Ru–PIND was synthesized in a single-step double ligand-exchange reaction. To a solution of $Ru(bpy)_2Cl_2$ (0.10 g, 0.20 mmol) in 8.0 ml freshly distilled ethylene glycol was added 0.24 g PIND (0.50 mmol) and the resulting mixture was stirred for 10 min before refluxing. The course of the ligand-exchange reaction was monitored by cyclic voltammetry. The orange reaction mixture was then poured slowly into 500 ml of rapidly stirred anhydrous ether. The precipitate was collected by suction filtration through a fine fritted funnel. The crude product was dissolved in 8−10 ml of water and was extracted twice with chloroform. The precipitate was further purified by crystallization from ethanol giving the pure product in 80% yield. The product showed a single pair of reversible redox waves at a gold electrode with an $E_{1/2}$ of 0.70 V in aqueous solution. To ensure a complete double ligand-exchange, a slight excess of PIND (10−25%) is required.

Biosensor preparation, hybridization and detection

The pretreatment and silanization of the ITO electrode were performed according to the method of Russell *et al.* (15). Oligonucleotide capture probes immobilization was carried out as follows: aldehyde-modified capture probes were denatured for 10 min at 90°C and diluted to a concentration of 0.50 μM in 0.10 M acetate buffer (pH 6.0). A 25 μl aliquot of the capture probes solution was dispensed onto the silanized electrode and incubated for 2−3 h at 20°C in an environmental chamber. After incubation, the electrode was rinsed successively with 0.10% SDS and water. The reduction of the imines was carried out by a 5 min incubation of the electrode in a 2.5 mg/ml sodium borohydride solution made of PBS/ethanol (3/1). The electrode was then soaked in vigorously stirred hot water (90−95°C) for 2 min, copiously rinsed with water and blown dry with a stream of nitrogen. To minimize non-hybridization-related PIND–Ru–PIND uptake and improve the quality and the stability of the biosensor, the capture probe coated electrode was immersed in an ethanolic solution of 2.0 mg/ml AUA for 3−5 h. Unreacted AUA molecules were rinsed off and the electrode was washed by immersion in stirred ethanol for 10 min, followed by a thorough rinsing with ethanol and water. The surface density of the immobilized capture probes, assessed electrochemically

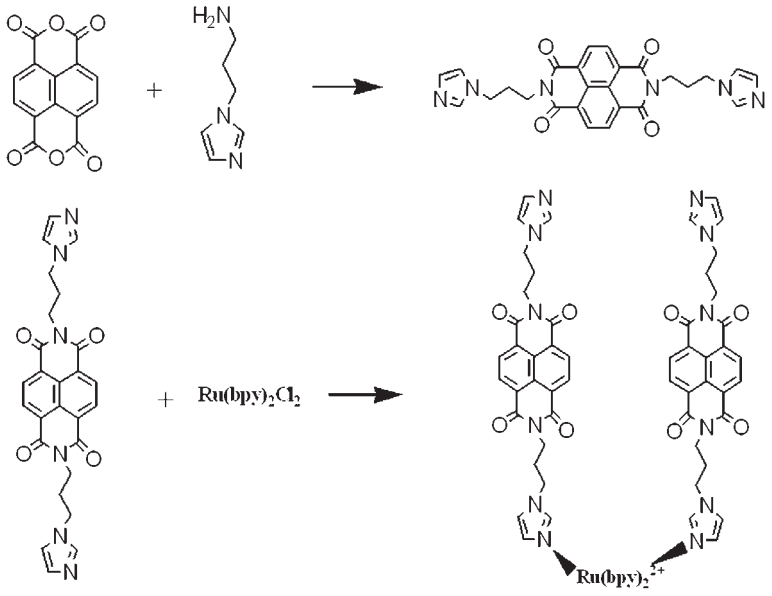

Scheme 1. Synthetic route to PIND-Ru-PIND bis-intercalator.

using Tarlov's method (16), was found to be in the range of $5-8 \times 10^{-12}$ mol/cm^2, i.e. 20–25% lower than that found at gold electrodes. This is probably due to a lower capture probe immobilization efficiency via chemical coupling. The hybridization of the target nucleic acid and its photoelectrochemical detection were carried out in three steps. First, the biosensor was placed in an environmental chamber maintained at 50°C. A 25 µl aliquot of hybridization solution containing the target nucleic acid was uniformly spread onto the biosensor and was then rinsed thoroughly with a blank hybridization solution at 50°C after 60 min of hybridization. PIND–Ru–PIND was attached to the hybridized target nucleic acid via *bis*-threading intercalation after 20 min incubation at 25°C with a 25 µl aliquot of 50–100 µM PIND–Ru–PIND in TE buffer (pH 6.0, adjusted with 10 mM HCl). It was then thoroughly rinsed with the TE buffer (pH 6.0). Photocurrent was measured at 0.10 V in 0.10 M $NaClO_4$.

RESULTS AND DISCUSSION

Intercalation with nucleic acids

To determine the mode of interaction of PIND–Ru–PIND with double-stranded DNA (dsDNA), UV-Vis spectrophotometry of PIND–Ru–PIND in the presence of increasing amounts of salmon sperm DNA was investigated. In the UV-Vis spectrophotometry, signatures of intercalative binding, where the fused planar aromatic ring system of a threading intercalator inserts itself between the base pairs of dsDNA, are hypochromism and red shifts. As shown in Figure 1A, the addition of DNA to PIND–Ru–PIND at a DNA base pair/PIND–Ru–PIND ratio of 5.0 resulted in an ~35% decrease and an ~3 nm red-shift of the naphthalene diimide (ND) absorption band at 364 and 385 nm. Similar phenomena were previously observed with ND having aliphatic tertiary amine side chains (17,18). The hypochromism of ND absorption band reached a plateau at the base pair/PIND–Ru–PIND ratio >5.0, and

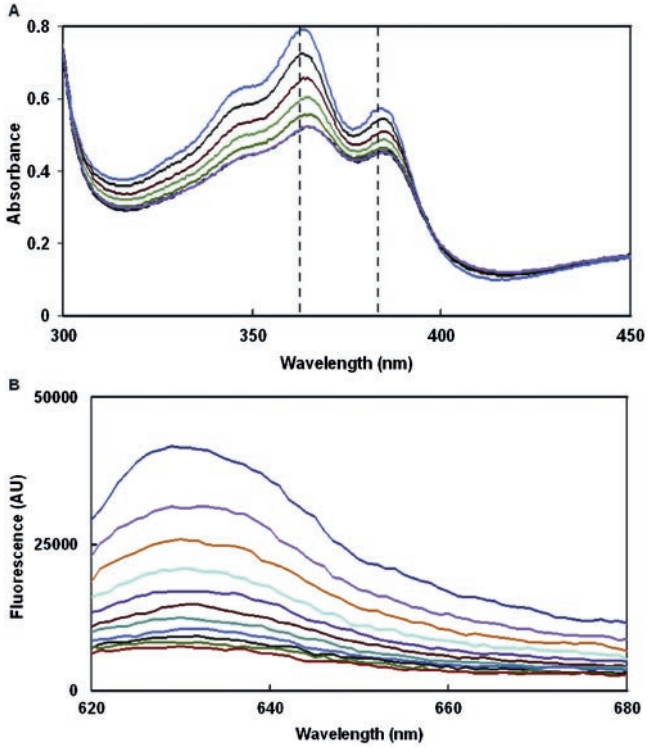

Figure 1. (**A**) UV-Vis absorption spectra of 25 µM PIND–Ru–PIND as a function of increasing concentration of salmon sperm DNA (in base pair). From top to bottom: 0, 25, 50, 75, 100, 125, 150 and 175 µM. (**B**) Competitive displacement fluorometric results of DNA binding property of PIND–Ru–PIND in 0.20 µM YOYO-3+0.50 µM DNA (in base pair). Tris buffer (20 mM; pH 6.0), PIND–Ru–PIND/YOYO-3 ratio from top to bottom: 0, 1/5, 2/5, 3/5, 4/5, 1/1, 6/5, 7/5, 8/5, 9/5 and 2/1.

a constant hypochromism was observed for ratios >5.0. A single clean isosbestic point was also observed at all DNA base pair/PIND–Ru–PIND ratios, suggesting that only one spectrally distinct PIND–Ru–PIND/DNA complex is present.

Both observations are qualitatively consistent with those observed for intercalating compounds, indicating that binding of PIND–Ru–PIND to dsDNA takes place by preferential intercalation.

Competitive displacement fluorometric assays were used to determine the apparent equilibrium constant (K_{app}) for PIND–Ru–PIND binding. The basis of this methodology involves the use of two intercalators, one fluorescent and the other non-fluorescent. The fluorescent intercalator first saturates the dsDNA. Then a second intercalator, in this case PIND−Ru–PIND, is introduced into the system with a gradual increase in concentration. Competitive binding leads to a loss of fluorescence because of the depletion of the DNA-bound fluorescent intercalator. A well-known *bis*-intercalator, YOYO-3, was chosen as our fluorescent indicator as it has been widely studied as an efficient DNA *bis*-intercalator and has a binding stoichiometry similar to that of PIND–Ru–PIND (19). More importantly, it possesses relatively little sequence preference and displays a 1000-fold fluorescence enhancement upon binding to dsDNA, providing sufficient sensitivity and good discrimination against the free YOYO-3 molecules in fluorescence measurement (19). K_{app} can be calculated using the equation: $K_{app} = K_{YOYO\text{-}3}\ xC_{YOYO\text{-}3}/C_{50}$ (20) where $K_{YOYO\text{-}3} = 1.5 \times 10^8\ M^{-1}$ for YOYO-3 binding to dsDNA (19) and C_{50} is the concentration of PIND–Ru–PIND at which 50% of an initially bound YOYO-3 is replaced by PIND–Ru–PIND. The binding constant K_{app} estimated from the experimental data (Figure 1B) was 4.0×10^8, corresponding to an ~700-fold enhancement over ND, paving the way to developing ultrasensitive nucleic acid biosensors.

Feasibility of photoelectrochemical detection of nucleic acids

The scheme for photoelectrochemical detection of nucleic acid through direct hybridization and formation of the nucleic acid/photoreporter adduct is similar to that of electrochemical detection (11). Briefly, prior to the test, a monolayer of oligonucleotide capture probes was immobilized onto the ITO electrode surface through chemical coupling. The electrode was then sequentially exposed to the target nucleic acid solution and the intercalator solution. Upon illumination, a photoelctrochemical response (photocharging current) was generated in the system followed by a discharging current when the illumination was off. Both charging and discharging currents correlate directly to the target nucleic acid concentration.

In the first hybridization test, a synthetic oligonucleotide was selected as our target nucleic acid. Upon hybridization at 50°C for 60 min, the target nucleic acid was selectively bound to its complementary capture probes and became fixed on the biosensor surface. PIND–Ru–PIND was brought to the biosensor via *bis*-threading intercalation during subsequent incubation with a 50 μM PIND–Ru–PIND solution. Typical cyclic voltammograms of the biosensor after intercalation are shown in Figure 2A. As shown in Figure 2A (trace 1), a considerably higher peak current was observed for the anodic process of the first cycle, indicating that a larger amount of electrons is involved in the oxidation process, most probably due to the electrocatalytic oxidation of the captured nucleic acid (guanine bases) (21–23). The peak current dropped significantly during the successive potential cycling and a steady-state voltammogram was attained after three cycles between 0 and 1.0 V (Figure 2A, trace 2). Extensive washing and potential cycling thereafter produced no noticeable changes, revealing that the intercalator is robustly bound to the dsDNA at the biosensor surface through *bis*-threading intercalation. Figure 2A (trace 3), is the voltammogram of an electrode coated with non-complementary capture probes (control biosensor) after the same treatments. Negligible redox activity at the redox potential of PIND–Ru–PIND was observed. These results clearly demonstrated that PIND–Ru–PIND selectively

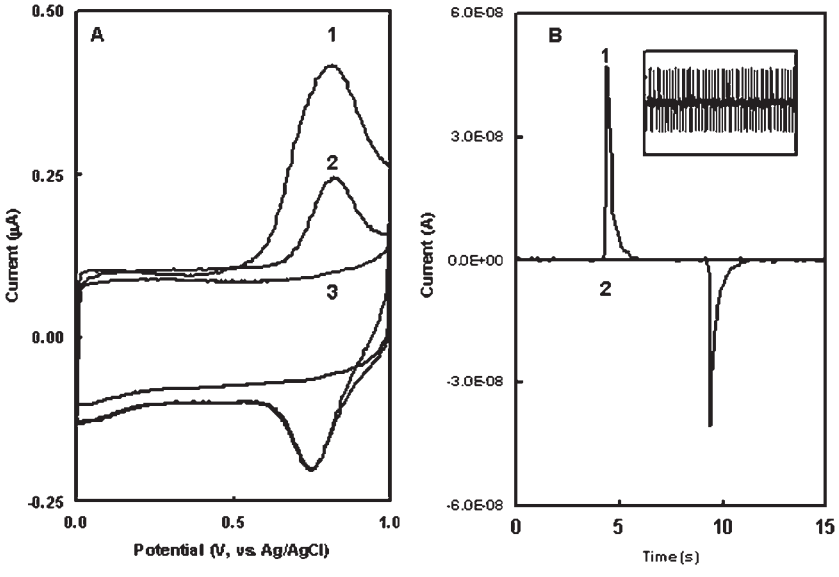

Figure 2. (**A**) Cyclic voltammograms of a 50 nM of target nucleic acid hybridized and PIND–Ru–PIND intercalated biosensor: (1) first scan, (2) third scan and (3) a control biosensor. Potential scan rate is 100 mV/s. (**B**) Photoelectrochemical responses of (1) the 25 nM target nucleic acid hybridized and PIND–Ru–PIND intercalated biosensor and (2) control biosensor. Inset: Stability test of the biosensor. Wavelength 490 nm, light intensity 22.4 mW/cm^2, applied potential 0.10 V.

interacts with dsDNA and the resulting dsDNA/PIND–Ru–PIND adduct has a very slow dissociation rate. Moreover, there is little non-hybridization related PIND–Ru–PIND uptake due to the presence of cationic amine on the biosensor surface, which paves the way for developing ultrasensitive nucleic acid biosensors. A plausible explanation for the high stability would be that, after the two ND groups have intercalated with the dsDNA, the bicationic $Ru(bpy)_2^{2+}$ group and the two protonated imidazole groups in PIND–Ru–PIND form ion-pairs with phosphates on the two sides of the dsDNA, significantly slowing down the dissociation process. Another possible mechanism of PIND–Ru–PIND uptake might be purely electrostatic interaction between the hybridized DNA and PIND–Ru–PIND. If this was the case, the control biosensor would produce a voltammogram with a peak current $\geqslant$50% of that of the biosensor and the peak currents of both biosensors would gradually decay towards zero (16). To further elucidate the role of electrostatic interaction in the biosensor, a neutral DNA analogue, a peptide nucleic acid with an identical sequence was employed. Voltammetric responses similar to those of target DNA were observed at both the biosensor and the control biosensor, suggesting that there is little contribution from the electrostatic effect. Consequently, the intercalated PIND–Ru–PIND can be used as a redox active indicator for direct voltammetric detection of nucleic acid. A detection limit of 0.50 nM and a dynamic range of 0.8–200 nM were obtained. The hybridization efficiency of ~32%, estimated at the high end of the dynamic range using the procedure proposed by Tarlov and co-workers (16) and YOYO-3 fluorescence assay, indicates that ~10% of the target nucleic acid was actually hybridized, which is comparable with that found in the literature (11,24,25). The number of intercalated PIND–Ru–PIND molecules was estimated from the charge under the steady-state voltammogram. Integration of the oxidation or reduction current peak at a low scan rate of $\leqslant$10 mV/s yielded a charge of 0.29 μC, resulting therefore from 3.0 pmol of active and intercalated PIND–Ru–PIND. This number represents <0.1% of PIND–Ru–PIND contained in the assayed droplet and a PIND–Ru–PIND/base pair ratio of 1/5–1/6, which is in a good agreement with that obtained in the UV-Vis experiments.

The possibility of utilizing the intercalated PIND–Ru–PIND as a photoreporter for the transduction of nucleic acid hybridization events was examined next. Figure 2B (trace 1) shows the photoelectrochemical response of the biosensor, after hybridization and treatment with PIND–Ru–PIND, as the illumination was turned on and off. The photocurrent generation consisted of two steps. An initial spike in photocurrent (photocharging) appeared promptly following the illumination, which was then followed by a quick decay to the background level. It took <2.0 s for the photocurrent to drop to the background level. This represents separations of photogenerated electron-hole pairs at the biosensor surface. Under positive bias, the holes 'move' to the biosensor–solution interface, while electrons 'sink' toward the substrate electrode. The quick decay of the photocurrent indicates that a major fraction of the electrons/holes are accumulated at the interface, instead of giving/capturing electrons to/from the electrolyte (26). When the light was turned off, a similar photocurrent transient behavior of the cathodic current (photodischarging) was observed. The cathodic current decayed with time from an initial maximum down to the background level within 2.0 s, caused by the recombination of the photogenerated electrons and holes at the biosensor surface. The photocharge/discharge cycle can be regenerated over 10^3 times in 60 min without noticeable decrease in its intensity. A portion of the regeneration experiment (50 cycles) is depicted in the inset in Figure 2B. In contrast, the control biosensor failed to capture any target nucleic acid and therefore no photoelectrochemical activity was observed upon illumination (Figure 2B, trace 2). It has been demonstrated that nucleic acid acts as a hole-generating biopolymer (27–29). Two limiting mechanisms, namely superexchange (30) and discrete hopping (31), have been proposed. Both mechanisms require a structural distortion of the nucleic acid double helix (32,33). The question of how charges migrate over long distance through nucleic acid is still a matter of controversial debate (27–36). Nonetheless, it has been generally accepted that the π-stack nucleic acid system has its unique electronic properties, differing significantly from other biopolymers such as proteins and carbohydrates. Charge generation, separation and recombination processes take place upon illumination (27–36). In a more recent report, photostimulated hole transport through dsDNA was observed (37). It was shown that the efficiency of hole transport is profoundly dependent on the sequence of the DNA and the potential bias. The magnitude of the photocurrent decreased sharply when the potential bias became less positive, approaching the background level at 0.0 V and leaving obviously only photogenerated charge separation in the system (37). Detailed mechanism of the PIND–Ru–PIND intercalation and photoelectrochemical response of the nucleic acid/PIND–Ru–PIND adduct is beyond the scope of this study. It will be elucidated in a forthcoming report.

Photocurrent action spectra, i.e. plots of the observed photoelectrochemical responses as a function of the wavelength of the incident light are shown in Figure 3. It can be seen that the photocurrent action spectrum of the hybridized and intercalated biosensor in the region of 400−600 nm (Figure 3, trace 2) coincides with the absorption spectrum of PIND–Ru–PIND (Figure 3, trace 3) with the highest photocurrent at 490 nm,

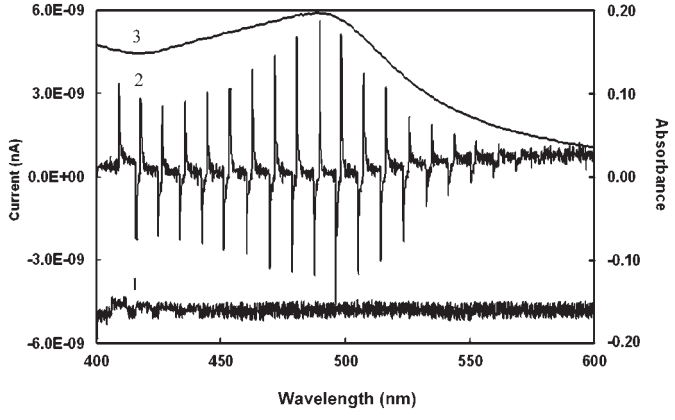

Figure 3. Photocurrent action spectra of (1) a control biosensor, (2) a 1.0 nM target nucleic acid hybridized and PIND–Ru–PIND treated biosensor and (3) UV-Vis absorption spectrum of 25 μM PIND–Ru–PIND in H_2O. Illumination was conducted with monochromatic light at a 10 nm interval. The photocurrent was collected at 0.10 V.

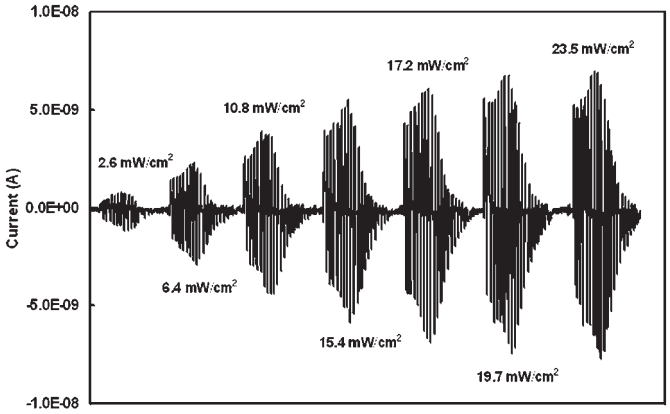

Figure 4. Dependence of photocurrent on the incident light intensity (400−600 nm) of a 1.0 nM nucleic acid hybridized and PIND–Ru–PIND intercalated biosensor at 0.10 V.

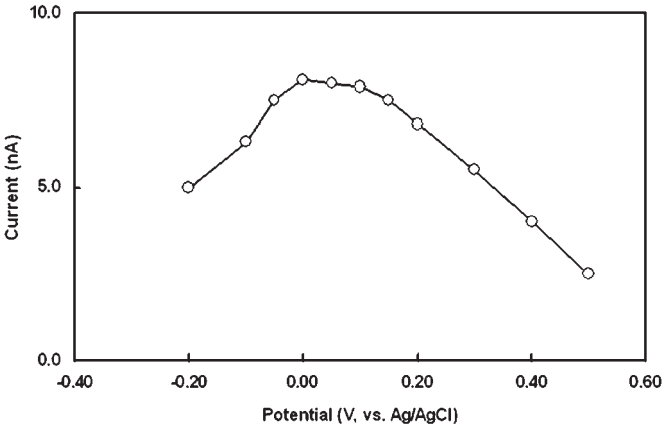

Figure 5. Dependence of photocurrent on the applied potential of a 1.0 nM target DNA hybridized and PIND–Ru–PIND treated complementary capture probe coated electrode. Illumination was conducted with a 23.1 mW/cm^2 monochromatic light beam of 490 nm.

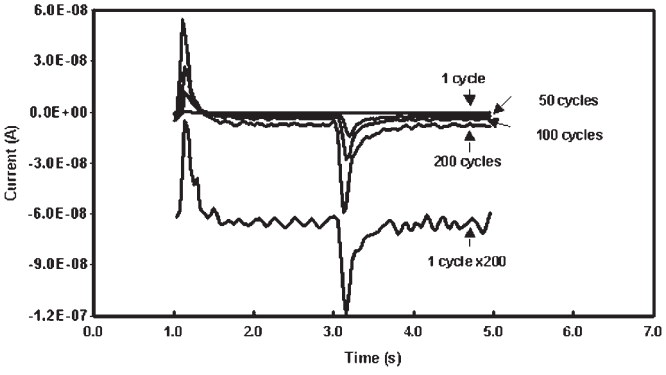

Figure 6. Photoelectrochemical response of multiple illumination cycles of a 100 pM target nucleic acid hybridized and PIND–Ru–PIND treated biosensor. Wavelength 490 nm, light intensity 22.8 mW/cm^2.

suggesting that PIND–Ru–PIND is indeed the photoactive element on the biosensor surface. This pattern of photocurrent was highly reproducible for numerous on−off illumination cycles. On the other hand, as in the case of voltammetry, in the absence of intercalated photoreporter, the control biosensor showed little photoactivity (Figure 3, trace 1). The minute anodic photocurrents observed in the region of 400−430 nm are mainly due to a suppressed photoelectrochemical activity of the substrate electrode (38).

As expected, the illumination intensity had a profound effect on the photocurrent. As shown in Figure 4, the photocharging/discharging current increased linearly with the incident light intensity up to 20 mW/cm^2 and leveled off at higher intensities. The linear relationship between the photocurrent and the incident light intensity suggests that the photogeneration of charge carriers is a monophotonic process (38,39). To attain a high sensitivity, the light intensity should be kept as high as possible.

Figure 5 depicts the dependence of photocurrent on the applied potential. The photocharging current increased gradually when the applied potential became less anodic. The increase in photocharging current with a less positive bias is due to the decrease in charge-collection efficiency, as the photogenerated charge carriers will be less efficiently transported to the electrode/electrolyte (37). The onset potential was found to be ~0.60 V. Above the onset potential, all photogenerated charge carriers are collected/lost in interfacial reactions. As the applied potential decreases, the fraction of the collected/lost charge carriers decreases. The amount of this fraction is practically independent of light intensity, which implies that it is only the efficiency with which the charge carriers are transported to or withdrawn from the electrode that limits the photocharging current.

In view of the extremely low dissociation rate of the nucleic acid/photoreporter adduct and the highly reversible photoelectrochemical response, a significant sensitivity enhancement is expected through integration of multiple illumination cycles, analogous to the approach routinely employed in spectroscopic techniques, such as ^{13}C NMR and ultrathin organic film FT-IR, in detecting very weak signals in a noisy background. As demonstrated in Figure 6, both the photocharging and the discharging current increased almost linearly with increasing number of illumination cycles, up to 10^3 cycles. Moreover, substantial reduction of the background noises was also obtained as random noises tend to cancel each other after integration over sufficiently large number of cycles.

Analytical applications in nucleic acid assays

The applicability of the photoelectrochemical approach in nucleic acid assays was subsequently tested on genomic samples. In this study, a full-length TP53 cDNA was used as calibration standard and was diluted to different concentrations with a pH 8.0 hybridization buffer before use. Analyte solutions with different concentrations of cDNA, ranging from 10 fM to 10 nM, were tested. For the control experiment, non-complementary capture probes were used in the biosensor preparation. As depicted in Figure 7A, the voltammetric data of TP53 cDNA agreed well with the voltammetric results obtained earlier and confirmed that the TP53 cDNA was successfully detected. However, attempts to detect TP53 cDNA at picomolar levels were unsuccessful. On the other hand, the photoelectrochemical approach offered a much better sensitivity. As shown in Figure 7B, a 1000-cycle integration generated a dynamic range of 50 fM–1.0 nM ($R^2 = 0.97$)

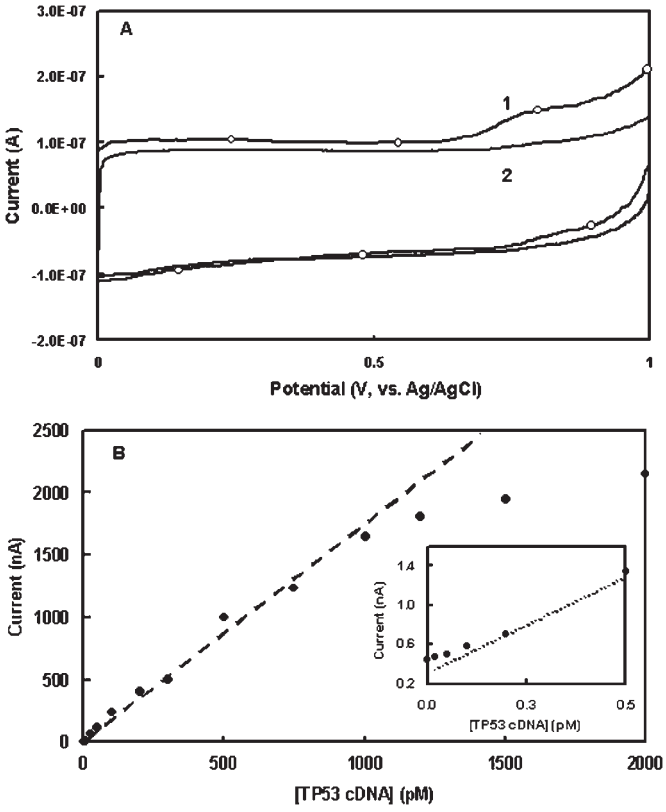

Figure 7. (**A**) Cyclic voltammograms of (1) a 2.0 nM of TP53 cDNA hybridized and PIND–Ru–PIND intercalated biosensor and (2) a control biosensor. Potential scan rate was 100 mV/s. (**B**) Photoelectrochemical responses of TP53 cDNA at different concentrations. Integration of 1000 cycles, wavelength 490 nm, light intensity 22.7 mW/cm^2. Inset: Photoelectrochemical responses at low concentration end.

with a relative SD of 13% at 5.0 pM (20 duplicates) and a detection limit of ~20 fM, a 10^4-fold sensitivity enhancement over voltammetry. It was noteworthy that the sensitivity is comparable to short oligonucleotides although a much less hybridization efficiency is expected (8,9). Theoretically, at the same molar concentration, the sensitivity should be roughly proportional to the hybridization efficiency provided that the lengths of capture probes are the same. But this trend was not observed in our experiments. To have a better understanding of the hybridization efficiency and PIND–Ru–PIND loading level, a series of voltammetric measurements were carried out with 1.0 nM TP53 after hybridization and after intercalation. It was shown that ~3.0 fmol of TP53 was hybridized. This number represents that ~0.21% of the surface-bound capture probes were actually hybridized, a much lower value than that of short oligonucleotides (20–50mer) reported in the literature (8,9,24,25). It is not surprising that the hybridization efficiency decreases drastically with the increasing size of the analyzed gene. In addition, the voltammetric experiments showed that an average of ~20 PIND–Ru–PIND molecules intercalated with the hybridized TP53. The substantial discrepancy between hybridization efficiency and PIND–Ru–PIND loading level suggest that some of the PIND–Ru–PIND molecules intercalated into the secondary structure of TP53 (40,41), further enhancing the sensitivity of this method.

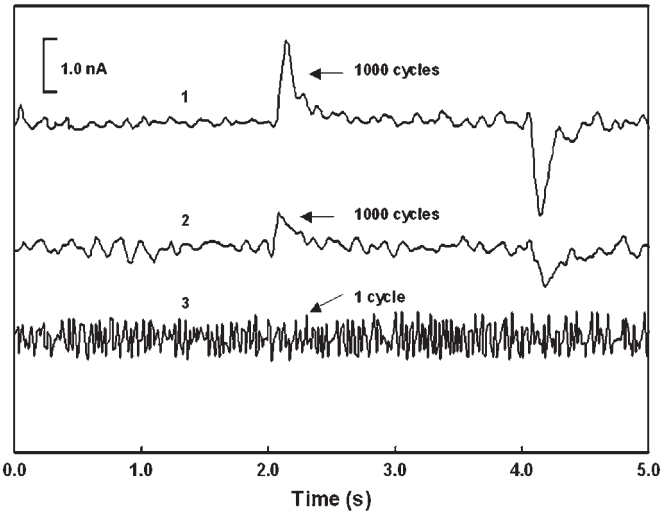

Figure 8. Photoelectrochemical responses of biosensors after hybridization and intercalation of 50 ng mRNA sample with capture probes (1) and (3) complementary, and (2) one-base mismatch to TP53. Wavelength 490 nm, light intensity 22.9 mW/cm^2.

The applicability of the photoelectrochemical approach was further evaluated with real-world samples, 50 ng of mRNA extracted from tissues, to determine the ability in detecting a specific gene in the mRNA mixture. Considering that there are ~30 000 genes in this mRNA pool, the actual detectable amount of any gene is at picograms (~subpicomolar) on average. As shown in Figure 8 (trace 1), the current increment for the biosensor coated with perfectly matched capture probe was in the range of 2.2–2.6 nA. If the fully complementary capture probes were replaced with mismatched probes (A↔T or G↔C mismatch in the middle of the capture probes), the current increment dropped by at least 60% to as low as 0.85 nA, when one base was mismatched (Figure 8, trace 2); and it was practically indistinguishable from the background noise when two bases were mismatched, readily allowing selective detection of genes in a complex nucleic acid mixture and discrimination between the perfectly matched and mismatched genes.

CONCLUSIONS

In summary, the successful adaptation of photoelectrochemistry in nucleic acid hybridization detection is demonstrated. The unique photoelectrochemical properties of the nucleic acid/PIND–Ru–PIND adduct provide a convenient route for quantification of target nucleic acids. The ultrahigh sensitivity of the biosensor described here enables the quantification of nucleic acids without a preamplification step. This nucleic acid detection method is of general applicability and is extendable to multiplexed nucleic acid assays. A logical extension of the photoelectrochemical procedure will be the fabrication of a photoelectrochemical biosensor array and the incorporation of the array into a fully automated microelectromechanical system coupled with a visible light source. Low noise potentiostats, capable of monitoring picoampere currents can also be built into the system. Thus, the photoelectrochemical instrumentation for DNA detection is likely to be smaller than that

of comparably sensitive non-electrochemical methods. Current efforts are focused on revealing the mechanism of the *bis*-intercalation and photoelectrochemical response and further improving the performance of the photoelectrochemical biosensor.

ACKNOWLEDGEMENTS

The authors would like to acknowledge financial support from IBN/A*STAR. Funding to pay the Open Access publication charges for this article was provided by IBN.

Conflict of interest statement. None declared.

REFERENCES

1. Kricka,L.J. (1995) *Nonisotopic Probing, Blotting and Sequencing*. 2nd edn. Academic Press Inc., San Diego, CA.
2. Edwards,M.C. and Gibbs,R.A. (1994) Multiplex PCR: advantages, development, and applications. *PCR Methods Appl*, **3**, S65–S75.
3. Baugh,L.R., Hill,A.A., Brown,E.L. and Hunter,C.P. (2001) Quantitative analysis of mRNA amplification by *in vitro* transcription. *Nucleic Acids Res*., **29**, e29.
4. Lizardi,P., Huang,X., Zhu,Z., Bray-Ward,P., Thomas,D. and Ward,D. (1998) Mutation detection and single molecule counting using isothermal rolling circle amplification. *Nature Genet*., **19**, 225–232.
5. Urdea,M.S., Running,J.A., Horn,T., Clyne,J., Ku,L.L. and Warner,B.D. (1987) A novel method for the rapid detection of specific nucleotide sequences in crude biological samples without blotting or radioactivity; application to the analysis of hepatitis B virus in human serum. *Gene*, **61**, 253–264.
6. Wiedorn,K.H., Kuhl,H., Galle,J., Caselitz,J. and Vollmer,E. (1999) Comparison of *in situ* hybridization, direct and indirect *in situ* PCR as well as tyramide signal amplification for detection of HPV. *Histochem. Cell. Biol*., **111**, 89–95.
7. Patolsky,F., Ranjit,K.T., Lichtenstein,A. and Willner,I. (2000) Dendritic amplification of DNA analysis by oligonucleotide-functionalized Au-nanoparticles. *Chem. Commun*., **12**, 1025–1026.
8. Xie,H., Zhang,C. and Gao,Z. (2004) Amperometric detection of nucleic acid at femtomolar levels with a nucleic acid/electrochemical activator bilayer on gold electrode. *Anal. Chem*., **76**, 1611–1617.
9. Xie,H., Yu,Y.H., Xie,F., Lao,Y.Z. and Gao,Z. (2004) A nucleic acid biosensor for gene expression analysis in nanograms of mRNA. *Anal. Chem*., **76**, 4023–4029.
10. Zhang,Y., Kim,H.H. and Heller,A. (2003) Enzyme-amplified amperometric detection of 3000 copies of DNA in a 10-μL droplet at 0.5 fM concentration. *Anal. Chem*., **75**, 3267–3269.
11. Tansil,N.C., Xie,H., Xie,F. and Gao,Z. (2005) Direct detection of DNA with an electrocatalytic threading intercalator. *Anal. Chem*., **77**, 126–134.
12. Armistead,P.M. and Thorp,H.H. (2000) Modification of indium tin oxide electrodes with nucleic acids: detection of attomole quantities of immobilized DNA by electrocatalysis. *Anal. Chem*., **72**, 3764–3770.
13. Gore,M.R., Szalai,V.A., Ropp,P.A., Yang,I.V., Silverman,J.S. and Thorp,H.H. (2003) Detection of attomole quantities of DNA targets on gold microelectrodes by electrocatalytic nucleobase oxidation. *Anal. Chem*., **75**, 6586–6592.
14. Napier,M.E., Loomis,C.R., Sistare,M.F., Kim,J., Eckhardt,A.E. and Thorp,H.H. (1997) Probing biomolecule recognition with electron transfer: electrochemical sensors for DNA hybridization. *Bioconjug. Chem*., **8**, 906–913.
15. Hedges,D.H.P., Richardson,D.J. and Russell,D.A. (2004) Electrochemical control of protein monolayers at indium tin oxide surfaces for the reagentless optical biosensing of nitric oxide. *Langmuir*, **20**, 1901–1908.
16. Steel,A.B., Herne,T.T. and Tarlov,M.J. (1998) Electrochemical quantitation of DNA immobilized on gold. *Anal. Chem*., **70**, 4670–4677.
17. Lokey,R.S., Kwok,Y., Guelev,V., Pursell,C.J., Hurley,L.H. and Iverson,B.L. (1997) A new class of polyintercalating molecules. *J. Am. Chem. Soc*., **119**, 7202–7210.
18. Yen,S.F., Gabbay,E.J. and Wilson,W.D. (1982) Interaction of aromatic imides with deoxyribonucleic acid. Spectrophotometric and viscometric studies. *Biochemistry*, **21**, 2070–2076.
19. Haugland,R.P. (1992) *Handbook of Fluorescence Probes and Research Chemicals*. Molecular Probes, Eugene, OR.
20. Jenkins,T.C. (1997) Optical absorbance and fluorescence techniques for measuring DNA–drug interactions. In Fox,K.R. (ed.), *Methods in Molecular Biology*. Humana Press Inc., Totowa, NJ, Vol. 90, pp. 195–218.
21. Mugweru,A.M. and Rusling,J.F. (2001) Catalytic square-wave voltammetric detection of DNA with reversible metallopolymer-coated electrodes. *Electrochem. Commun*., **3**, 406–409.
22. Wang,B. and Rusling,J.F. (2003) Voltammetric sensor for chemical toxicity using $[Ru(bpy)_2poly(4\text{-vinylpyridine})_{10}Cl)]^+$ as catalyst in ultrathin films. DNA damage from methylating agents and an enzyme-generated epoxide. *Anal. Chem*., **75**, 4229–4235.
23. Mugweru,A. and Rusling,J.F. (2002) Square wave voltammetric detection of chemical DNA damage with catalytic poly(4-vinylpyridine)-$Ru(bpy)_2^{2+}$ films. *Anal. Chem*., **74**, 4044–4049.
24. Caruso,F., Rodda,E., Furlong,D.N., Niikura,K. and Okahata,Y. (1997) Quartz crystal microbalance study of DNA immobilization and hybridization for nucleic acid sensor development. *Anal. Chem*., **69**, 2043–2049.
25. Satjapipat,M., Sanedrin,R. and Zhou,F. (2001) Selective desorption of alkanethiols in mixed self-assembled monolayers for subsequent oligonucleotide attachment and DNA hybridization. *Langmuir*, **17**, 7637–7644.
26. Salvador,P. and Gutierrez,C. (1984) Analysis of the transient photocurrent-time behaviour of a sintered n-$SrTiO_3$ electrode in water photoelectrolysis. *J. Electroanal. Chem*., **160**, 117–130.
27. O'Neill,M.A. and Barton,J.K. (2002) Effects of strand and directional asymmetry on base-base coupling and charge transfer in double-helical DNA. *Proc. Natl Acad. Sci. USA*, **99**, 16543–16550.
28. Wagenknecht,H.A. (2003) Reductive electron transfer and transport of excess electrons in DNA. *Angew. Chem. Int. Ed. Engl*., **42**, 2454–2460.
29. Takada,T., Kawai,K., Cai,X.C., Sugimoto,A., Fujitsuka,M. and Majima,T. (2004) Charge separation in DNA via consecutive adenine hopping. *J. Am. Chem. Soc*., **126**, 1125–1129.
30. Turro,N.J. and Barton,J.K. (1998) Paradigms, supermolecules, electron transfer and chemistry at a distance. What's the problem? The science or the paradigm *J. Biol. Inorg. Chem*., **3**, 201–209.
31. Giese,B. (2000) Long-distance charge transport in DNA: the hopping mechanism. *Acc. Chem. Res*., **33**, 631–636.
32. Gary,B. and Schuster,G.B. (2000) Long-range charge transfer in DNA: Transient structural distortions control the distance dependence. *Acc. Chem. Res*., **33**, 253–260.
33. Wan,C., Fiebig,T., Kelly,S.O., Treadway,C.R., Barton,J.K. and Zewail,A.H. (1999) Femtosecond dynamics of DNA-mediated electron transfer. *Proc. Natl Acad. Sci. USA*, **96**, 6014–6019.
34. O'Neill,M.A., Dohno,C. and Barton,J.K. (2004) Direct chemical evidence for charge transfer between photoexcited 2-aminopurine and guanine in duplex DNA. *J. Am. Chem. Soc*., **126**, 1316–1317.
35. Lewis,F.D., Letsinger,R.L. and Wasielewski,M.R. (2001) Dynamic of photoinduced charge transfer and hole transport in synthetic DNA hairpins. *Acc. Chem. Res*., **34**, 159–170.
36. Beljonne,D., Pourtois,G., Ratner,M.A. and Bredas,J.L. (2003) Pathways for photoinduced charge separation in DNA hairpins. *J. Am. Chem. Soc*., **125**, 14510–14517.
37. Okamoto,A., Kamei,T., Tanaka,K. and Saito,I. (2004) Photostimulated hole transport through a DNA duplex immobilized on a gold electrode. *J. Am. Chem. Soc*., **126**, 14732–14733.
38. Tansil,N.C., Xie,H. and Gao,Z. (2004) Photoelectrochemical behavior of oxalate at an indium tin oxide electrode. *J. Phys. Chem. B*, **108**, 16850–16854.
39. Segui,J., Hotchandani,S., Baddou,D. and Leblanc,R.M. (1992) Photoelectric properties of ITO CDs chlorophyll-A Ag heterojunction solar cells. *J. Phys. Chem*., **95**, 8807–8812.
40. Eddy,S.R. (2001) Non-coding RNA genes and the modern RNA world. *Nature Rev. Genet*., **2**, 919–929.
41. D'Erchia,A.D., Pesole,G., Tullo,A., Saccone,C. and Sbisa,E. (1999) Guinea pig p53 mRNA: identification of new elements in coding and untranslated regions and their functional and evolutionary implications. *Genomics*, **58**, 50–64.